Three-dimension spectral characteristics of low-frequency Zonal Flow in the edge plasma of HL-2A tokamak

A.D. Liu[1], T. Lan[1], H.L. Zhao[1], C.X. Yu[1], L.W. Yan[2], J.Q. Dong[2], W.Y. Hong[2], K.J. Zhao[2], J. Qian[2], J. Cheng[2], D.L. Yu[2], Q.W. Yang[2]

[1]Department of Modern Physics, University of Science and Technology of China, Hefei Anhui 230026, China

[2]Southwestern Institute of Physics, P. O. Box 432, Chengdu, Sichuan 610041, China

E-mail address of main author: lad@mail.ustc.edu.cn

Abstract. The low-frequency Zonal Flow (LFZF), coexisting with the geodesic acoustic mode (GAM) was observed at the edge of HL-2A tokamak plasmas using four Langmuir probe arrays. It is identified as a low-frequency coherent mode peaking near zero frequency and broadening several kilohertz on the power spectral density (PSD) of the floating potential fluctuations. Besides the poloidal and toroidal axisymmetry, the radial wavenumber-frequency spectra of the LFZF was firstly estimated. The three-dimensional wavenumber-frequency spectral characteristics: $k_\theta = k_\phi \simeq 0$, $\bar{k_r}\rho_i = 3.3 \times 10^{-2}$ with the full width at half maximum $\Delta k_r \rho_i = 0.19$, are almost consistence with the theoretical predications and simulation results. The radial spectra showing that the LFZF packages propagate both outwards and inwards with a small net value outward, resulting in smaller phase shifts between two probe tips separated radially at the LFZF frequency than the GAM frequency. The envelope and the bispectrum analysis of the poloidal velocity fluctuations both reveal that the interaction between the LFZF and the ambient turbulence (AT) is as similar as that between the GAM and the AT, suggesting the same generation mechanism. But the differences are: the coherent coefficients between the LFZF and the envelope of the AT are smaller than that between the GAM and the AT, and the intensity of the tri-wave interactions including the LFZF is also much smaller than that including the GAM. These phenomena may both caused by the small amplitude of the LFZF in the edge region.

1. Introduction

Zonal flows[1], which are believed to play a crucial role in regulating the turbulence level and the turbulent transport, become a concerned issue in magnetically confined fusion plasmas over the last decade [2][3][4]. Two kinds of zonal Flow have been identified in toroidal magnetized plasma, i.e., a residual flow with a low (near zero) frequency, also called stationary zonal flows, and the oscillatory one with a higher frequency called geodesic acoustic mode zonal flow (GAMZF) caused by toroidal effects. Many characteristics have been confirmed in experiments, especially for the GAMZF, which could be identified more easily. Besides the pioneer work on edge plasma of DIII-D using the phase-contrast imaging (PCI) [5], the symmetry feature of the low-frequency Zonal Flow (LFZF) in the core plasma has been measured directly on the DIII-D by the beam emission spectroscopy (BES) [6][7] and on the CHS by the heavy ion beam probes (HIBP) [8]. There are also some indirect measurements showing the signature of the LFZF, such as the changement of nonlinear coupling of the bispectra or the envelope modulations [9][10][11] and the reduction of fluctuation-driven particle flux [12]. The overview of the experiments of zonal flows could be seen in [13]. In this paper, we describe the observation of the coexistence of the LFZF and GAMZF, and the first complete three-dimension spectral structure of the LFZF in the edge plasma of tokamak. The interaction between the LFZF, GAMZF and AT is also analyzed.

2. Experimental Setup

The experiments were carried out on the HuanLiuqi-2A (HL-2A) in the limiter configuration with the major radius $R = 1.65m$ and minor radius $a = 0.40m$. The experimental condition was the Ohmic

heated deuterium plasma with following typical parameters: plasma current $I_p = 160 \sim 180kA$, toroidal magnetic field $B_\phi = 1.4T$, line-averaged density $\bar{n}_e = (1 \sim 3) \times 10^{19} m^{-3}$, and safety factor at the limiter position $q_a = 3.5 \sim 4.0$. In this discharge condition, MHD activities are very weak, which can not interfere the detection of the LFZF and GAM. Measurements in the edge plasma ($r/a \geq 0.9$) were performed using two radially moveable Langmuir probe systems, as shown in Fig.1. The first probe system consists of three arrays, one (marked as B) of which is located in the outer midplane and the others (marked as A and C) are located symmetrically about the outer midplane in the same poloidal cross-section of the torus and poloidally separated by $d_\theta = 5.0cm$. The second probe system is composed of one probe array (marked as D) which is located $130cm$ toroidally (along $\overrightarrow{B}_\phi$) with respect to the first system in the outer midplane. Except for the probes in the array B which was used as a triple probe for measuring electron temperature as well as density and floating potential, all other probes were used to measure the floating potential. There are three steps in the array D for measuring the radial electric field, and the velocity of the poloidal $E \times B$ flows calculated as $\tilde{v}_\theta = -\tilde{E}_r / B_\phi$. All the signals were sampled by 12-bit digitizers at a sampling rate of 1MHz, which gave the Nyquist frequency of $f_N = 500kHz$.

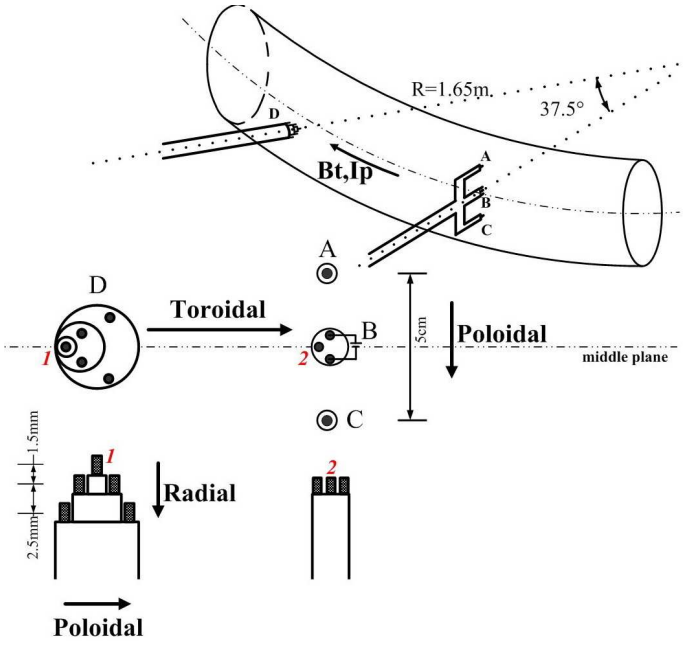

Fig. 1: The arrangement of experiments and the structures of four probe arrays. The probe tips marked as 1 and 2 are used to estimate radial structures of the LFZF and GAM.

3. Experimental results

3.1 Three-dimension spectral structures

The power spectral density (PSD) of potential fluctuations ($\tilde{\phi}_f$) with different frequency resolutions, along with their correlation coefficients and mode number spectra are shown in Figure 2. The PSD was estimated as an ensemble average for a stationary interval of $\sim 500ms$, and before fast fourier transform the linear trend of every realization has been removed to eliminate the contamination induced by the effects of slow movement of bulk plasma or changes in plasma parameters. In addition to the AT feature in the high frequency range of $> 20kHz$, the spectra exhibit two distinct spectral features: a coherent mode peaked at the frequency $\sim 8.5kHz$ with a full width at half-maximum of $\sim 3.5kHz$ and a low frequency broadband (from zero extending up to $3kHz$) feature with the tendency of peaking near zero frequency as increasing the frequency resolution from $1kHz$ to $0.125kHz$. We can see that both features have high coherencies and phase shifts of zero from Fig.2(b) and (c). The poloidal and toroidal mode numbers with statistic errors are listed in Table I for the low frequency broadband feature (from $0.5kHz$

Table I. Poloidal and toroidal mode numbers of $f = 0.5kHz \sim 3kHz$ and $f = 8.5kHz$.

	$0.5kHz$	$1kHz$	$1.5kHz$	$2kHz$	$2.5kHz$	$3kHz$	$8.5kHz$
m	0.43 ± 0.25	0.39 ± 0.29	0.31 ± 0.31	0.36 ± 0.33	0.36 ± 0.34	0.08 ± 0.39	0.04 ± 0.24
n	0.04 ± 0.06	0.02 ± 0.07	0.01 ± 0.08	0.07 ± 0.09	0.1 ± 0.1	0.05 ± 0.1	0.14 ± 0.04

to $3kHz$) and the coherent mode at $8.5kHz$ respectively, both smaller than one. The low frequency broadband feature can be regarded as a poloidally and toroidally symmetric mode of $m = 0$ and $n = 0$, and is consistent with the theoretical prediction and simulation result [14] for the LFZF. The coherent mode at $\sim 8.5kHz$ has been identified to be GAMZF, as similar to the previously observation [15][16], and will be analyzed further for comparing with the LFZF.

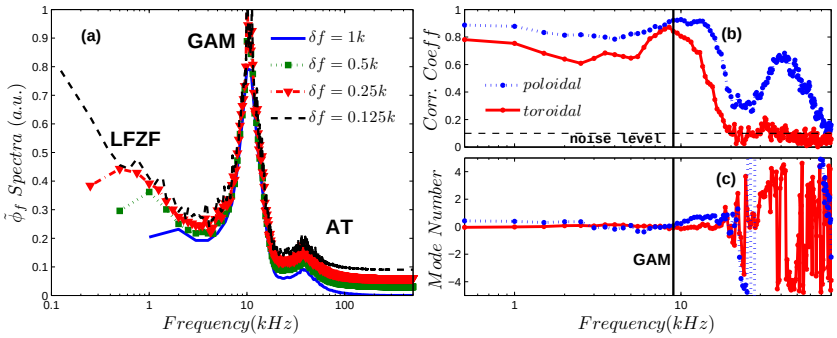

Fig. 2: (a) PSD of $\tilde{\phi}_f$ under different frequency resolution (small vertical shifts added for clarity). (b) The spectra of coherent coefficients and (c) mode numbers between two $\tilde{\phi}_f$s separated poloidally and toroidally.

The radial spectral structure can be characterized with the local wavenumber-frequency spectrum $S(k_r, f)$ calculated using the two-point cross-correlation technique [17]. Figure3 illustrate the contour plot of the $S(k_r, f)$ spectrum (frequency range: $0.5kHz \sim 20kHz$) for $\tilde{\phi}_f$ as well as the conditional spectrum $s(k_r/f) = S(k_r, f)/S(f)$, where $S(f) = \Sigma_k S(k, f)$, for the LFZF at the frequency $0.5kHz$ and GAMZF at the frequency $8.5kHz$. The wavenumber resolution of spectra here is chosen to be $\delta k = 1.06cm^{-1}$, which is a tradeoff between reduction in the variance of the spectral estimate and loss of the wavenumber resolution for a given realization number. The $1.5mm$ radial separation is the inverse proportion to the range of the measured radial wavenumber, which is from $-\pi/0.15 \simeq -21cm^{-1}$ to $21cm^{-1}$. Thus the smaller the radial distance, the more realizations needed. It should be noticed that the radial correlation of potential fluctuations are measured by the two probe of tips 1 in the array D and tip 2 in the array B (marked in Fig.1) with radial and toroidal separations of $1.5mm$ and $130cm$ respectively to minimize the impact of the AT whose toroidal correlation length is much less than zonal flows. A phase shift measured by the two probes is composed of both radial and toroidal components, i.e. $\Delta\theta_{12}(f) = k_r(f)d_r + k_\phi(f)d_\phi$. Because the toroidal phase shift for both the LFZF and GAM is zero as described above and its contribution is negligible, the cross-phase $\Delta\theta_{12}(f)$ can be used to estimate the radial wavenumber for the LFZF and GAM.

It can be seen that the spectra of $S(k_r, f)$ and $s(k_r/f)$ for the GAMZF are single-peaked at a positive k_r value, indicating that the GAMZF propagates radially outwards with little inward propagation component (positive k_r represent propagating outward in this paper). In contrast, the spectra for the LFZF appear to be two peaks at approximately sym-

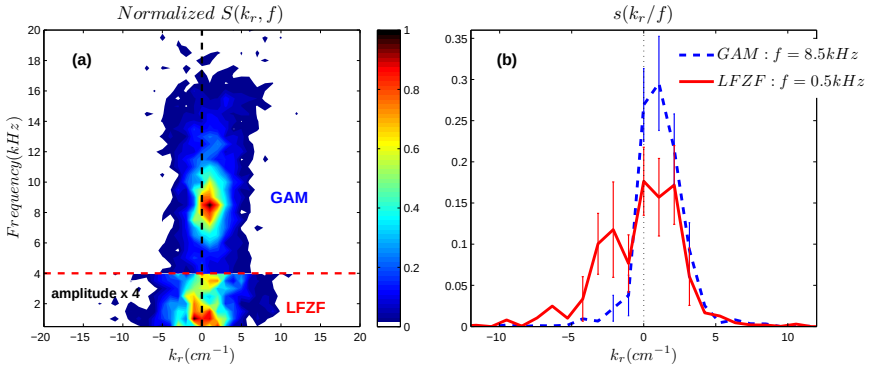

Fig. 3: (a) $S(k_r, f)$ below $20kHz$(the part under the red dashed line is multiplied by 4 for better comparison). (b) $s(k_r/f)$ for $f = f_{GAM}$ and $f = 0.5kHz$.

metric positive and negative values $k_r \sim \pm 1.06cm^{-1}$ with a small imbalance in the positive and negative components, which is similar to that observed in the edge plasma of DIII-D [5]. This observation implies that the LFZF propagates in both the radial inward and outward directions with a small net outward. These observations present a striking contrast to the characteristic radial structure of the GAMZF. The spectral averaged wavenumber and wavenumber width estimated from $s(k_r/f)$ are respectively $\bar{k}_r = 0.55cm^{-1}$ and $\Delta k_r = 3.2cm^{-1}$, which corresponds to $\bar{k}_r\rho_i = 3.3 \times 10^{-2}$ and $\Delta(k_r\rho_i) = 0.19$. This is in the range for the LFZF expected by theory and simulations [14]. The finite radial structure of the LFZF can also be inferred from the changes of the time-lag cross-correlations between lowpass-filtered $\tilde{\phi}_f$s measured by the probe tips 1 and 2 with increasing radial separation, as shown in Fig.4. The picture display that the correlation coefficients in the LFZF frequency range of $0 - 2.5kHz$ decreases monotonically with increasing separation. We can roughly estimate the radial correlation length of $0.5cm < L_r^{LFZF} < 1cm$, which corresponds to approximately ten times ion cyclotron radius and is shorter than that of the GAM. In brief, the LFZF has a smaller radial wavenumber and decays more quickly than the GAM, giving possible explanations to the radial phase shifts measuring by BES in DIII-D (Fig.3 in [6]).

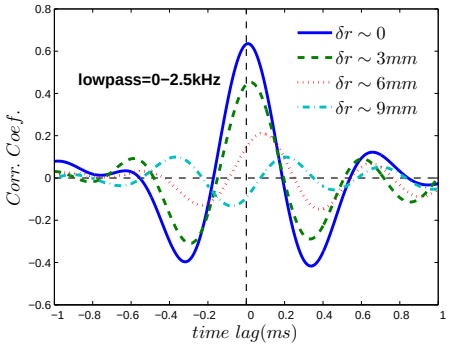

Fig. 4: The correlation coefficients vs. time lags, showing the radial propagation and finite decorrelation length of the LFZF.

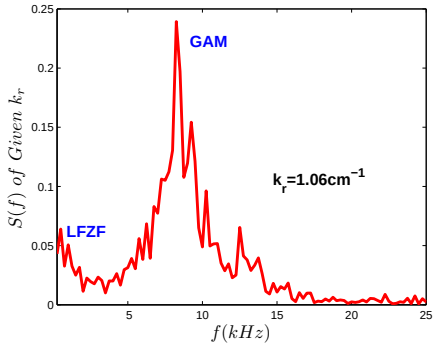

Fig. 5: $S(k_r, f)$ at $k_r = 1.06cm^{-1}$.

Figure5 shows the power spectrum of ZFs at a given wavenumber of $k_r = 1.06cm^{-1}$, deduced from $S(k_r, f)$. The spectral features for both the LFZF and GAMZF can be seen clearly from the figure: The LFZF spectrum has a peak at $\sim 0.5kHz$ with a width of $\sim 1.5kHz$, corresponding to the correlation time of $0.7ms$ which is much longer than that of AT ($\sim 10\mu s$). The GAMZF spectrum has a peak at $\sim 8.5kHz$ with a width of $\sim 3kHz$. These features, especially the LFZF intensity is much smaller than that of the GAMZF here, are in sharp contrast to the simulation result of toroidal ITG turbulence for typical core plasmas [14] and observed results [7][8] in the core plasma which reveal that the LFZF intensity is much larger than the GAMZF. This difference is consistent with the theoretical prediction that the ZF intensity is dominated by the LFZF in the core region and by the GAM in the edge region [18][19][20] because of different damping mechanisms and this may be the reason that the LFZF is more difficult to be observed than the GAM in the edge region.

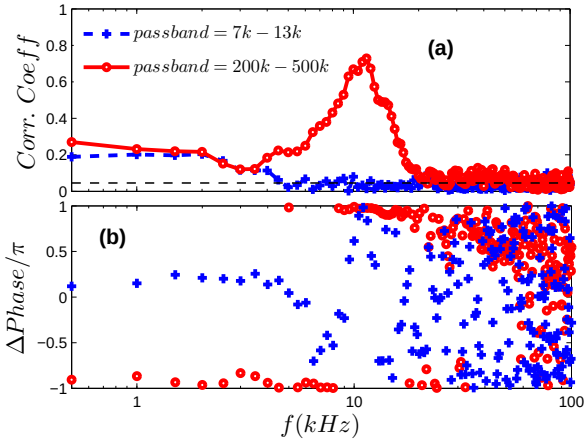

Fig. 6: (a) Coherent coefficient and (b) cross-phase spectra between $\tilde{E}_r$ and the envelope of filtered $\tilde{E}_r$ using two different bandpass filters.

3.2. Envelope Analysis

In order to investigate the nonlinear interaction between the LFZF, GAMZF and AT, the envelope analysis [21] is used. The envelope is defined as the modulus of the analytic signal composed of the original signal and that whose complex phase angles are shifted by $\pi/2$. According to the theory of zonal flow generation based on parametric or modulational instability, the generation of zonal flows is accompanied by the envelope modulation of AT [22][23][24]. If it is the case, the information on the nonlinear interaction between the ZFs and AT should be embodied in the envelope. Thus, the cross-correlation between fluctuations and the envelope of fluctuations can used to identify the nonlinear coupling between ZFs and AT. The correlation coefficients and cross-phase spectra between $\tilde{E}_r$ and the envelopes of the bandpass in the frequency ranges $f = 200 - 500kHz$ (referred to the AT envelope) and $f = 7 - 13kHz$ (referred to the GAMZF envelope) are shown in Fig.6(a) and (b). The coherencies clearly show that there are significant correlations between the LFZF and the envelopes of both the AT and GAMZF with a finite coherency of ≥ 0.2, in addition to the strong correlation between the GAMZF and the AT envelope. This result indicates that the AT envelope is modulated by both the LFZF and GAMZF, and the GAMZF envelope may also be modulated by the LFZF. Moreover, the modulation amplitude induced by the LFZF is a factor of $\sim (3-4)$ smaller than that by the GAMZF, which is consistent with the LFZF amplitude shown in Fig.5. The cross-phase spectra illustrate that the AT envelope modulation delays both the LFZF and GAMZF by about π radian and the GAMZF envelope modulation is almost in phase with the LFZF. According to the analysis to the mechanism of the envelope modulation, cross-phase spectra near π strongly suggest that the envelope modulation process is dominantly caused by the amplitude modulation effect during the ZFs generation and the phase modulation effect caused by the Doppler shift is subordinate [25]. Thus, the cross-phase in Fig.6(b) implies that both the LFZF and GAMZF gain or lose energy synchronously with the decrease or increase of the turbulence energy. Because both the LFZF and GAMZF are the ZF- eigenmodes they should not be able to interact directly. The GAMZF envelope modulation by the LFZF appeared in the coherence spectrum may not be an indicator of the direct nonlinear interaction between them. Therefore, these results strongly suggest that both the LFZF and GAMZF are simultaneously generated in the energy-conserving nonlinear interaction with the AT, as is predicted by the theory of zonal flow generation based on the parametric or modulational instability.

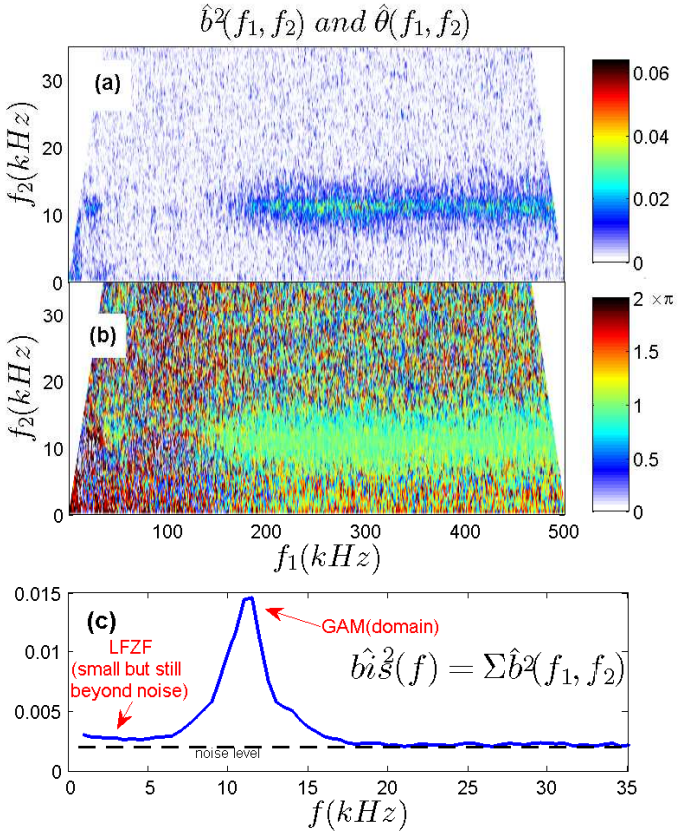

Fig. 7: (a) The squared self-bicoherence $\hat{b}^2_{E_r}(f_1,f_2)$, (b) the self-biphase $\hat{\theta}_{E_r}(f_1,f_2)/\pi$ and (c) the the summed squared bicoherence $\hat{bis}^2_{E_r}$.

3.3 Bispectrum

Other method to quantify the strength of the nonlinear three-wave interaction between ZFs and AT is

the bispectrum analysis [26]. The auto-bicoherence and biphase are defined as follows: $\hat{b}^2(f_1,f_2) = |\hat{B}(f_1,f_2)|^2/[\langle|\tilde{E}_r(f_1)\tilde{E}_r(f_2)|^2\rangle\langle|\tilde{E}_r(f_3)|^2\rangle]$ and $\hat{\theta}(f_1,f_2) = tan^{-1}(\mathrm{Im}(\hat{B}(f_1,f_2))/\mathrm{Re}(\hat{B}(f_1,f_2)))$, where $\hat{B}(f_1,f_2) = \langle\tilde{E}_r(f_1)\tilde{E}_r(f_2)\tilde{E}_r(f_3 = f_1+f_2)\rangle$ is the auto-bispectrum. In this definition, the bicoherence quantifies the fraction of power at the frequency $f_3 = f_1 + f_2$ due to the three-wave coupling. The biphase measures the degree of the phase coherence among three waves at frequencies f_1, f_2 and f_3 and if a coherent phase relationship exists due to nonlinear coupling, the biphase, averaged over many realizations, will be a constant value and the bicoherence will reach a finite value beyond the noise level. Figure7(a) and (b) show the contour plots of them, computed with a resolution of $0.5kHz$ and ensemble averaging over 480 realizations. Because of the symmetry property of auto-bicoherence, both spectra are plotted within the triangle $0 \le f_2 \le f_N/2$ and $f_2 \le f_1 \le f_N - f_2$. From Fig.7(a) It can be seen that the values of $\hat{b}^2(f_1, f_{GAM} = 11kHz)$ are clearly much larger than that at other frequencies, which indicates that a strong nonlinear coupling exists in the wave triads $(f_1, f_{GAM}, f_1 + f_{GAM})$. The values of $\hat{b}^2(f_1, f_{LFZF} = 0 - 3kHz)$, though much smaller than $\hat{b}^2(f_1, f_{GAM} = 11kHz)$, are still larger than the statistical uncertainties. The biphase given in Fig.7(b) shows a weak dependence on f_1 with constant values of $\sim \pi$ over the f_2 frequency range of the LFZF and the GAMZF, verifying that the nonlinear interactions between zonal flows (LFZF and GAMZF) and AT are both coherent. This implies that nonlinear interactions also occur among resonant wave triads $(f_1, f_{LFZF}, f_1 + f_{LFZF})$ but coupling strength appears to be weaker than that among frequency triads $(f_1, f_{GAM}, f_1 + f_{GAM})$. This difference of the bicoherences at frequencies of the LFZF and GAMZF is illustrated in Fig.7(c), where the summed bicoherence $\hat{bis}^2(f) = \Sigma_{f=f_1+f_2}\hat{b}^2(f_1,f_2)/N(f)$ is shown and $N(f)$ is the number of triads satisfying $f = f_1 + f_2$. According to the theoretical interpretation of the bispectrum analysis for the drift wave-zonal flow system [27][28], the summed bicoherence at the frequency of zonal flows is proportional to the ZF amplitude. Thus the difference in the summed bicoherences at the LFZF and GAMZF frequencies could also be explained by the smaller intensity of the LFZF.

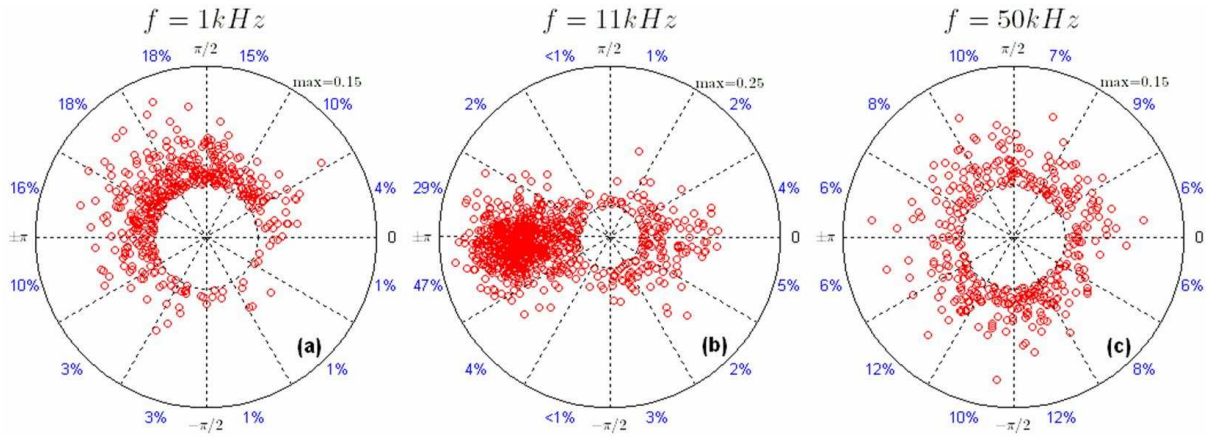

Fig. 8: Distributions of the bicoherences of three kinds of resonant wave triads: (a) including the LFZF, (b) including the GAMZF and (c) including $50kHz$.

In order to show the contrast of the nonlinear couplings of the LFZF and GAMZF clearly, the distributions of the bispectrum of all the triads contributed to three given frequency f are shown in Fig.8 respectively: $f = 1kHz$(referred to the LFZF), $f = 11kHz$(referred to the GAMZF) and $f = 50kHz$(referred to other frequency). Every point in the polar coordinates (ρ, ϕ) represents the bispectrum of one wave triad (f_1, f_2, f): the distance to the origin point $\rho = \hat{b}(f_1, f_2)$, the azimuth angle $\phi = \hat{\theta}(f_1, f_2)$ and the points whose ρ below the noise level are not included (the dash circle in the center means noise level). The numbers around the outmost solid circle are the percentages of the number of the points located in the corresponding 30^0 pie sections, thus if the three waves at f_1, f_2 and f have statistically independent random phases, the distribution of $\phi = \theta_f - \theta_{f_1} - \theta_{f_2}$ will be random and these numbers should all around $1/12 = 8.33\%$. The formula $max =?$ at the top right corner shows the maximum among all points, i.e. the maximum of all $\hat{b}(f_1, f_2)$ in the figure. Figure8(b) shows a typical concentrative distribution and

Fig.8(c) shows an approximate random distribution while Fig.8.(a) seems like an intermediate stage, corresponding to three kinds of resonant wave triads interactions: strongly coherent, weakly coherent and incoherent. Our next work is to estimate a precise mathematic model to describe the differences more quantitatively.

4. Summary

In summary, the LFZF has been observed to be coexisted with the GAMZF in the edge plasma for the first time. The three-dimensional spectral features of the LFZF are identified to have many characteristics expected for the stationary zonal flow. In particular, the observation of the toroidal and poloidal symmetry provides the first conclusive evidence for the LFZF axisymmetry of theoretical predictions. The radial wavenumber spectra exhibit that the LFZF packet radially propagates both outwards and inwards with a net outward. In addition, both the LFZF and GAMZF are found to modulate the intensity of the potential fluctuations with the anti-phase relation. This result strongly suggests that both the LFZF and GAMZF are simultaneously generated in the energy-conserving nonlinear interaction with AT. All the results demonstrate that the LFZF intensity is much smaller than that of the GAMZF in the higher q edge region, in agreement with expectations from theory and simulation.

References

[1] A. Hasegawa, C. G. Maclennan and Y. Kodama, Phys. Fluids **22**, 2122 (1979).

[2] M.N. Rosenbluth and F.L. Hinton, Phys. Rev. Lett. **80**, 724 (1998)

[3] Z. Lin *et al.*, Science 281, 1835 (1998).

[4] P.H. Diamond *et al.*, Plasma Phys. Control. Fusion **47**, R35 (2005).

[5] S. Coda, M. Porkolab and K.H. Burrell, Phys. Rev. Lett. **86**, 4835 (2001).

[6] G.R. Mckee *et al.*, in *Proceedings of the 21th IAEA Fusion Energy Conference* (Chengdu, China, 2006), EX/2-3.

[7] D.K. Gupta *et al.*, Phys. Rev. Lett. **97**, 125002 (2006).

[8] A. Fujisawa *et al.*, Phys. Rev. Lett. **93**, 165002 (2004).

[9] R.A. Moyer *et al.*, Phys. Rev. Lett. **(**87), 135001-1 (2001).

[10] G.S. Xu *et al.*, Phys. Rev. Lett. **91**, 125001 (2003).

[11] Y. Nagashima *et al.*, Phys. Rev. Lett. **95**, 095002 (2005).

[12] M.G. Shats, W.M. Solomon and H. Xia, Phys. Rev. Lett. **90**, 125002-1 (2003).

[13] A. Fujisawa *et al.*, Nucl. Fusion **47** S718 (2007).

[14] T. S. Hahm *et al.*, Plasma Phys. Control. Fusion **42**, A205 (2000).

[15] K.J. Zhao *et al.*, Phys. Rev. Lett. **96**, 255004 (2006).

[16] T. Lan *et al.*, Plasma Phys. Control. Fusion **50**, 045002 (2008).

[17] J.M. Beall *et al.*, J. Appl. Phys. **53**, 3933 (1982).

[18] K. Hallatschek, Phys. Rev. Lett. **93**, 065001-1 (2004).

[19] K. Hallatschek, Plasma Phys. Control. Fusion **49**, B137 (2007).

[20] B. Scott, Phys. Lett. A **320**, 53 (2003).

[21] D. Gabor, J. Inst. Electr. Eng., **93**,429 (1946).

[22] L. Chen, Z. Lin and R.B. White, Phys. Plasmas **7**, 3129 (2000).

[23] L. Chen, R.B. White and F. Zonca, Phys. Rev. Lett. **92**, 075004-1 (2004).

[24] P.H. Diamond *et al*, Nucl. Fusion **41**, 1067 (2001).

[25] T. Lan *et al* Phys. Plasma, **15** 056105 (2008).

[26] Y.C. Kim *et al.*, IEEE Trans. Plasma Sci. **PS-7**, 120 (1979).

[27] P.H. Diamond *et al.*, Phys. Rev. Lett. **84**, 4842 (2000).

[28] K. Itoh *et al.*, Phys. Plasmas **12**, 102301 (2005).